Volume 4, Number 2, 2011. pp. 79-86

Jordan Journal of Physics

ARTICLE

Investigation of the Experimental Effects on the Quality of the Rapid Acquisition Pair Distribution Function (RA-PDF) Data

Ahmad S. Masadeh

Department of Physics, University of Jordan, Amman 11945, Jordan.

Received on: 3/5/2011; Accepted on: 13/10/2011

Abstract: Series of experiments have been carried out to investigate the quality of the recently developed rapid acquisition atomic pair distribution function (RA-PDF) method, which combines the uses of high energy X-rays and an image plate area detector. Image plate data for simple elements (C, Mg, Al, Si, Ni, Cu, Zn, Ag, and Pb) have been analyzed, using (RA-PDF) technique. The affect of undiscriminated Compton and fluorescence is investigated for a wide range of materials with atomic Z numbers ranging from 6 (Carbon) and 82 (Pb). We find the RA-PDF method is capable of obtaining high quality PDFs where quantitatively reliable structure information can be extracted.

Keywords: Rapid acquisition atomic pair distribution function; Total scattering, RA-PDF, X-ray scattering.

PACS: 61.46.Df, 61.10.-i, 78.66.Hf, 61.46.-w.

Introduction

Modern scientifically and technologically important materials are becoming increasingly disordered. The knowledge of the atomic structure, in three dimensions, of such materials is prerequisite for understanding their properties. In the literature, there are powerful tools for studying long-range atomic structure (crystallography) and local structure (EXAFS, NMR), but very little for probing the intermediate structure scale of 110 nm. The atomic pair distribution function (PDF) method has emerged as a powerful tool to study the atomic structure at different length scales. The PDF is used to characterize the local structure of crystalline and nano-crystalline materials [1, 2], in additional to its traditional use on glass, liquids, and amorphous materials [3, 4].

Being a real space approach assuming long-range order is not preserved, the PDF method is growing in popularity as the conventional crystallographic analysis becomes less effective for increasingly disordered materials [5–8]. For PDF experiments, short wavelength X-rays or neutrons are used. Modern third generation synchrotron and spallation neutron sources are capable of delivering short wavelength photons (neutrons) for wide momentum transfer (Q) range giving the PDF technique with much improved high real-space resolution [1, 2]. For PDF measurements, sufficient counting statistics are needed. The required measurement time for each experiment is determined by the amount of sample in the beam (in neutron case), its scattering power, and X-ray/neutron flux available. One barrier for wide spread PDF applications has been the long data collection time (8 to 10 hours) with conventional PDF method, while the recently developed rapid acquisition PDF (RA-PDF) method [9] opens up the horizon for new possibilities by significantly lowering this barrier. In early proof-of-principle study [9], the RA-PDF method is

Corresponding Author: Ahmad S. Masadeh. **Email**: ahmad.masadeh@ju.edu.jo

shown to reduce the data collection time by three to four orders of magnitude, and give high quality PDFs with good reproducibility. The RA-PDF method benefits from 2D data collection by coupling high energy X-rays with an image plate (IP) area detector. The usage of IP area detector expedites data collection without compromising the measured reciprocal space range.

More recent, the RA-PDF method has been successfully applied to quantitatively measure the strain in nanoparticles [10], local distortions in Ti_2Sb [11], characterizing mesomorphous and amorphous active pharmaceutical ingredients [12], phase transitions in α-AlF_3 [13], and in-situ time resolved study of nano-ceria [13]. The RA-PDF method is expecting to extend into broad scientific areas, which will benefit the local structure PDF analysis, and will help significantly in our understanding of structures at the atomic level.

The use of IP area detector for quantitative PDF analysis subject to careful scrutinies imposed by the introduced experimental effects. One major concern is the lack of energy resolution intrinsic to the IP. The measured counts are the sum of elastic, Compton, and fluorescence intensities, while only elastic signal (exponentially decreasing with Q) is useful to PDF analysis. Extraction of the elastic component can be very challenging at high momentum transfer Q where Compton scattering dominates especially for low-Z elements.

Fluorescence can be very significant for medium to high Z elements when the X-ray energy is not far enough above the absorption edges. In addition to that, the IP response is energy dependent making the situation more complicated. IP data collection also exposed to high background scattering levels mostly coming from the rather long direct beam flight path in air after the sample. The lack of collimation in front of the IP also raises the issue of background scattering from sample environments, such as low temperature measurements with cryostat, studies with pressure anvil cells.

In this paper, we perform a series of experiments to investigate the experimental effects on the quality of the RA-PDF data and the accuracy of the structural information obtained.

Materials with the atomic Z numbers ranging from 6 to 82 are measured to systematically study the effect of Compton and fluorescence contributions to the total signal. The data for elements with medium atomic number Z, ($12 \leq Z \leq 30$), and high−Z, ($47 \leq Z \leq 82$), could be analyzed and modeled, up to $Q_{max} = 30.0$ Å^{-1}, and resulted in high quality PDFs. This study reveals that RA-PDF method is capable of obtaining high quality PDFs where quantitatively reliable structure information can be extracted.

Experiments

Data acquisition

In the recent developed RA-PDF experiments, great efforts have been taken to reduce the scattering back ground. Extensive Pb shielding before the sample is usually loaded, which is proved to be very helpful. The collimation between the Pb shield and the sample (if there is some considerable gap) proved to be rather effective too. The IP camera is repeatedly adjusted to be aligned to be orthogonal to the incident beam.

The IP center is also moved to be on the incident beam. Those aligning steps are necessary in order to minimize the errors during later data corrections, e.g. the incident angle (used in oblique incident angle dependence correction, read on for details) relative to the IP is assumed to be the same as 2θ.

The diffraction experiment was performed at 6IDD beamline at the advance photon source (APS) at Argonne National Laboratory, Argonne, IL (USA). Image plate camera (Mar345), of a usable diameter of 345 mm, mounted orthogonal to the beam path with sample to detector distance of 178.4 mm, was used to collect the data at room temperature. The energy of the X-ray used is 98.0 keV. The samples (C, Mg, Al, Si, Ni, Cu, Zn, Ag, and Pb) were purchased from Alfa Aesar and were used as received.

Fine powders of all samples were measured in flat plate transmission geometry with thickness 1.0 mm packed between kapton tapes. The air-sensitive samples were handled in a nitrogen-filled glove bag.

Data processing

Determination of S(q) from the raw data

All raw 2D data, like the one shown in Fig. 1, were integrated and converted to intensity versus 2θ using the software Fit2D [14], where 2θ is the angle between the incident and scattered X-rays. The integrated data were normalized by the average monitor counts. The data were corrected using standard methods [1, 2] to obtain the total scattering structure function, $S(Q)$, and the PDF, $G(r)$.

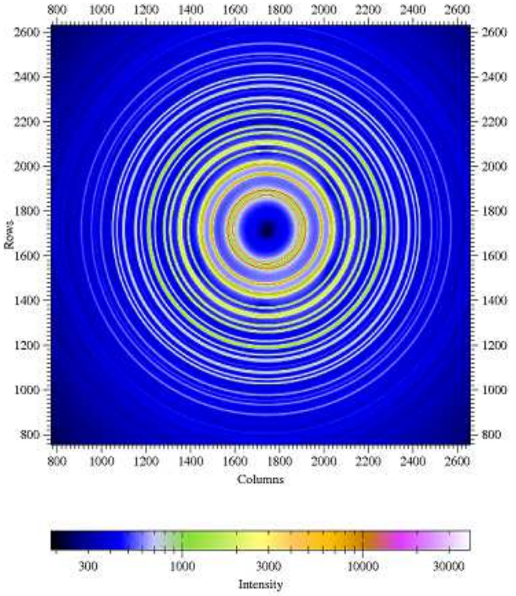

FIG. **1.** Two dimensional contour plot from the Mar345 Image Plate Detector. The XRD data are from nickel powder measured at ambient conditions. The concentric circles represent intersections of different colors with the area detector (Debye-Scherrer rings). The sample was contained in a flat plate, 1.0 mm thickness, irradiated volume 0.25 mm^3, beam size 0.5× 0.5 mm^2. The small dark area in the center of the image is a shadow cast by the beam stop assembly.

Calculation of G(r) from S(q)

Program PDFgetX2 [15] was used to process X-ray powder diffraction data to obtain the experimental PDF, $G(r)$. Standard corrections were made to the raw data to account for experimental effects such as Compton, fluorescence, and oblique incident angle dependence to obtain the normalized total scattering structure function, $S(Q)$. The PDF, $G(r)$, is obtained by a Fourier transformation according to Eq. 2.

In the Fourier transform step to get from $S(Q)$ to the PDF, $G(r)$, the data are truncated at a finite maximum value of the momentum transfer, $Q = Q_{max}$. Different values of Q_{max} may be considered. Here a Q_{max} = 30 Å^{-1} was found to be optimal. Q_{max} is optimized such as to avoid large termination effects and to reasonably minimize the introduced noise level as signal to noise ratio decreases with Q value. More details about the IP corrections are described in this section

The atomic PDF analysis of X-ray and neutron powder diffraction data is a powerful method for studying the structure of locally distorted materials. [1, 2, 8, 16–18] Recently, it has been explicitly applied to study the structure of discrete nanoparticles. [18–22] The PDF method can yield precise structural information at different length scales, provided that special care is applied to the measurement and to the method used for analyzing the data. The atomic PDF, $G(r)$, is defined as

$$G(r) = 4\pi r\,[\rho(r) - \rho_0]\ , \tag{1}$$

where $\rho(r)$ is the atomic pair-density, ρ_0 is the average atomic number density and r is the radial distance. [23] The PDF yields the probability of finding pairs of atoms separated by a distance r. It is obtained by a sine Fourier transformation of the reciprocal space total scattering structure function $S(Q)$, according to

$$G(r) = \frac{2}{\pi}\int_0^\infty Q[S_\alpha(Q) - 1]\sin(Qr)\,dQ\ , \tag{2}$$

where $S(Q)$ is obtained from a diffraction experiment. This approach is widely used for studying liquids, amorphous and crystalline materials, and has recently been applied to nanocrystalline materials. [2]

Extraction of the structural information from G(r).

Structural information was extracted from the PDFs using a full-profile real-space local-structure refinement method [24] analogous to Rietveld refinement. [25] We used the program PDFfit [26] to fit the experimental PDFs. Starting from a given structure model and given a set of parameters to be refined, PDFfit searches for the best structure that is consistent with the experimental PDF data. The residual function (R_w) is used to quantify the agreement of the calculated PDF from model to experimental data

$$R_w = \sqrt{\frac{\sum_{i=1}^{N} w(r_i)[G_{obs}(r_i) - G_{calc}(r_i)]^2}{\sum_{i=1}^{N} w(r_i) G_{obs}^2(r_i)}}. \qquad (3)$$

Here the weight $\omega(r_i)$ is set to unity which is justified because in $G(r)$ the statistical uncertainty on each point is approximately equal. [27, 28]

The structural parameters of the model were unit cell parameters, isotropic atomic displacement parameters (ADPs). Non structural parameters that were refined were a correction for the finite instrumental resolution, (σ_Q), low-r correlated motion peak sharpening factor (δ), [29, 30] and scale factor.

Description of X-ray PDF data analysis using IP area detector

Data analysis of IP data involves more steps. As the raw data coming off the IP are two dimensional (concentric Debye-Sherrer rings in our case of powder diffraction) images, program FIT2D [31] was first used to integrate around the rings to obtain the one dimensional scattering intensity versus 2θ equivalent to an angle dispersive scan. The integrated data were then normalized by the total incident beam flux during that exposure(s). Once we have the sample and background data, they can be used in PDFgetX2 [15] to obtain the $G(r)$. However, additional corrections are necessitated due to the nature of the IP data collection, as explained in the following.

Incident angle dependence this correction accounts for the angular dependence of the scattered photon effective path length in the IP phosphor layer [32], as a direct result of its incomplete absorption of the scattered photons. This correction becomes very significant at high X-ray energies and large incident angles (both present in RA-PDF analysis). Two parameters are used here, scattered photon absorption coefficient of the IP phosphor layer and the incident angle (= 2θ). The X-ray energy used in our experiments is highly penetrating with the absorption coefficient less than 1%.

Energy dependence of the IP response The counts of the IP is proportional to the X-ray energy stored in its phosphor layer, and thus depends on both the absorption coefficient per incident photon and the photon energy. This energy dependence of the IP response was found to decrease slowly with increasing photon energy with few discontinuities at low energies [33]. No correction of this nature is necessary for the elastically scattered photons as they have the same energy at all angles. However, the Compton scattering does not conserve the photon energies which monotonously decrease with increasing scattering angle. Here we use an empirical analytical form to approximate the energy dependence of the detection efficiency. The used analytical formula can be either linear or quadratic while ensuring the detection efficiency decreases with energy.

Fluorescence background the contribution from fluorescence can be very significant when the X-ray energy is not too far above the constituent elements' absorption edge(s). The angular dependence of the fluorescence is constant before self absorption correction. The magnitude of the fluorescence is used as an adjustable parameter during data processing. In principle, its intensity can be estimated from theoretical cross section tables. However, as the energy of fluorescence is usually well separated from both Compton and elastic scatterings, the interpolated energy dependence of the IP response causes the estimation less accurate.

Results and Discussion

The experimental reduced structure functions, $F(Q)$, and the corresponding PDFs, $G(r)$, for Cu, Zn, C and Pb samples are shown in figures 2- 5, respectively. Ideally, the $F(Q)$ would asymptote to zero with increasing Q value. A quick visual check reveals that the data quality varies rather considerably with the atomic Z number. Our data show that for low Z element, like carbon, shown in Fig. 4, extraction of the elastic component can present a challenge at high momentum transfer Q where Compton scattering dominates. For the high Z element, like lead, shown in Fig. 5, the contribution from fluorescence is found significant since the used X-ray energy is not too far above the measured-element absorption edge(s). The used X-ray energy is 98.0 keV where the Pb K-absorption edge is 88.0 keV. The obtained lattice parameters are slightly higher than the widely accepted values, for all the systems reported in Tables 1 and 2, due to systematic errors in the calibrated sample-detector distance. However, the refined lattice parameters from all elements reproduce their literature values fairly well; see (Table 1 and 2). This can be taken as an evidence of the accuracy of (RA-PDF) methods.

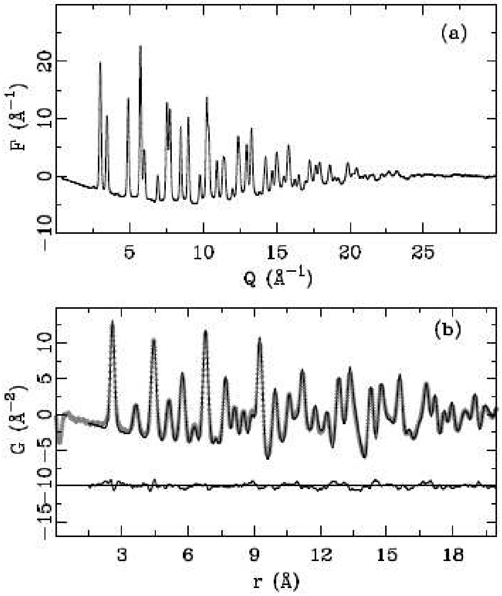

FIG. 2. (a) The experimental reduced structure function $F(Q) = Q\ (S(Q) - 1)$ for Cu. (b) The experimental $G(r)$ obtained by Fourier transforming the data in (a) (solid dots) and the calculated PDF from refined structural model (solid line). The difference curve is shown offset below.

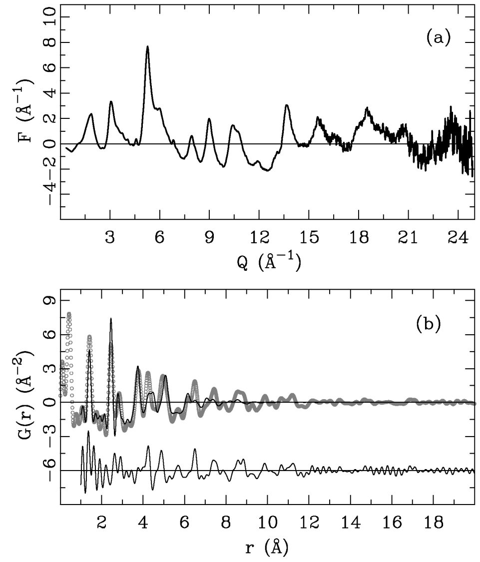

FIG. 4. (a) The experimental reduced structure function $F(Q) = Q\ (S(Q) - 1)$ for C. (b) The experimental $G(r)$ obtained by Fourier transforming the data in (a) (solid dots) and the calculated PDF from refined structural model (solid line). The difference curve is shown offset below.

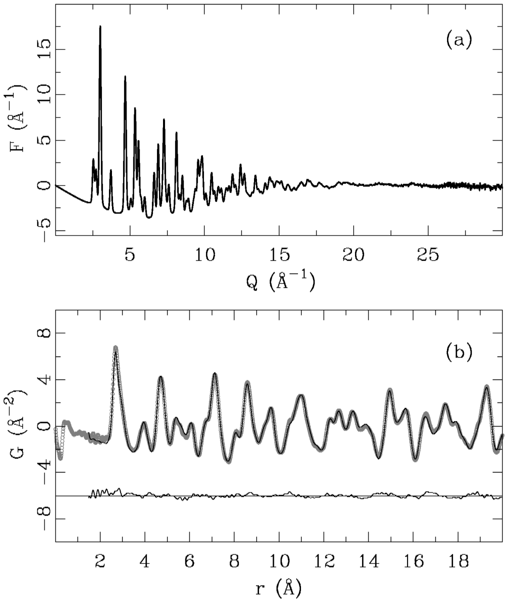

FIG. 3. (a) The experimental reduced structure function $F(Q) = Q\ (S(Q) - 1)$ for Zn. (b) The experimental $G(r)$ obtained by Fourier transforming the data in (a) (solid dots) and the calculated PDF from refined structural model (solid line). The difference curve is shown offset below.

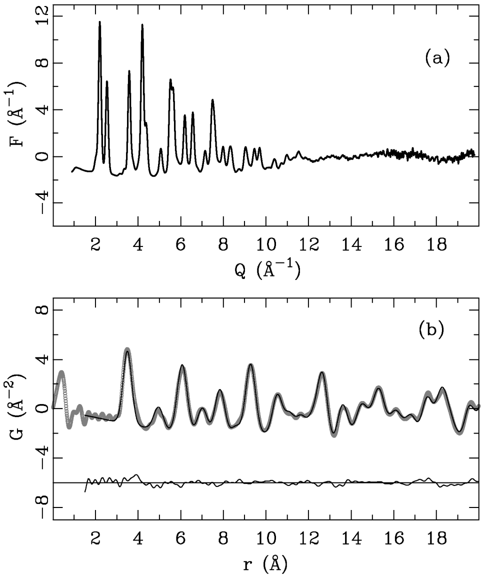

FIG. 5. (a) The experimental reduced structure function $F(Q) = Q\ (S(Q) - 1)$ for Pb. (b) The experimental $G(r)$ obtained by Fourier transforming the data in (a) (solid dots) and the calculated PDF from refined structural model (solid line). The difference curve is shown offset below.

TABLE 1. The result of the refined parameter values from the measured simple elements with cubic unit cell.

	Z	a(Å)$_{\text{literature}}$	a(Å)	U_{iso}(Å^2)	Rwp
Pb	83	4.95	4.968(2)	0.0104(1)	0.14
Ag	47	4.09	4.102(2)	0.0095(1)	0.10
Cu	29	3.61	3.627(2)	0.0074(1)	0.10
Ni	28	3.52	3.534(2)	0.0051(1)	0.09
Si	14	5.43	5.437(2)	0.0064(1)	0.13
Al	13	4.05	4.069(2)	0.0115(1)	0.11

TABLE 2. The result of the refined parameter values from the measured simple elements with a hexagonal unit cell.

	Z	a, c (Å)$_{\text{literature}}$	a, c(Å)	U_{iso}(Å^2)	Rwp
Zn	30	2.66, 4.95	2.67(1), 4.961(1)	0.0157(1)	0.09
Mg	12	3.21, 5.21	3.217(1), 5.221(1)	0.0162(1)	0.12
C	6	2.47, 6.79	2.447(1), 6.79(1)	0.0058(1)	0.32

Data collection with image plate can be subjected to quite high background. Part of the data analysis process is subtracting this background from the data. A scale factor close to unity suggests that uncertain background intensities have been subtracted successfully. From the results shown in Fig. 6, the value of the average scale factor for medium-Z and high-Z elements are 0.893 and 0.816, respectively, but for low-Z elements it is 0.30. The scale factor for medium and high-Z elements is close to 1.0. This suggests the data corrections for these data have been applied successfully. However, for low-Z element data, like carbon, there is a challenge in analyzing the data, even with lowering Q_{max} value down to 20.0 Å^{-1}. The best value for the scale factor could be obtained, in case of carbon, is 0.30, for Q_{max} = 20.0 Å^{-1}.

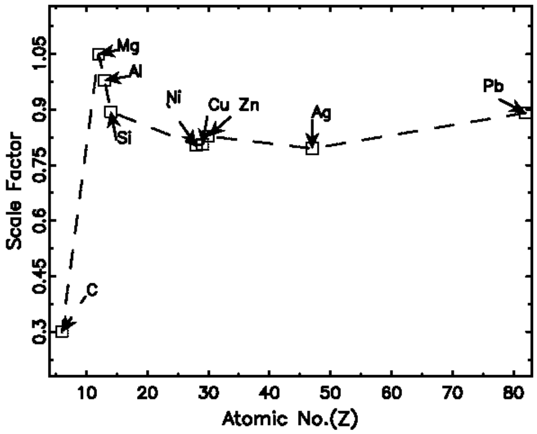

FIG. 6. Scale factor vs. atomic number (Z). All the data have Q_{max} = 30.0 Å^{-1}, except Pb and C they have Q_{max} 20 and 25 Å^{-1}, respectively.

All the PDFs from elements with cubic structure (Pb, Ag, Cu, Si, Ni, and Al) show highly acceptable qualities. For example, the Cu PDF, $G(r)$, data with Q_{max} = 30.0 Å^{-1}, Fig. 2, appears to have minimal systematic errors (unphysical features), which appear as small ripples before the first PDF peak at r = 2.55 Å. The structural model (space group *Fm-3m*) was readily refined, in the three dimensions real space, and gave excellent agreement with data as evident from the very small difference curve. The values of the weighted-profile R-value (R_{wp}) are listed in Table 1 and Table 2, with average value of R_{wp} 0.11, noting that a value of 0.10 indicates excellent agreement for PDF refinement. As can be seen from the R_{wp} value for cubic structure elements (Al, Ni, Cu, and Ag) has small fluctuation around the average of them 0.08 by σ = 0.008, which indicates in this Z −range ($13 \leq Z \leq 47$) the R_{wp} value (which is excellent) for that type of structure isn't influenced by the atomic number Z. However, for high−Z elements like Pb the obtained R_{wp} value is 0.32, for Q_{max} = 30.0Å^{-1}. The agreement factor (R_{wp}) for the Pb is the worst, due to the contribution of fluorescence signal, which is very significant since the used X-ray energy (98.0 keV) is not too far above the Pb K-absorption edge (88.0 keV). For high Z elements, the measured total counts are the sum of elastic, fluorescence intensities, while only elastic signal (exponentially decreasing with Q) is useful to PDF analysis. Extraction of the elastic component can be very challenging at high momentum transfer Q where fluorescence intensity dominates. Hence, the R_{wp} value is expected to improve as lowering the Q_{max} value.

The R_{wp} value for the Pb in Table 1 obtained for $Q_{max} = 20.0$ Å^{-1}, and it is 0.14.

For the elements with hexagonal structure (Zn and Mg), the PDFs show highly acceptable qualities, and the obtained R_{wp} value are listed in Table 2, with average value of R_{wp} 0.11. It is worth to notice that the fit of cubic structure model, Cu (Z = 29), Fig. 2, was comparable to the fit with hexagonal structure model, Zn (Z = 30), Fig. 3. The results suggest that elements with different structure models, but very close Z number, are expected to have the same PDF data quality. This can be seen from the difference curve bellow in figures Fig. 2 and Fig. 3, where Cu shows smaller differences as Zn, indicating that cubic structure data has same fitting quality as hexagonal. Noticing that both of them have almost the same atomic number (Z).

Weakly scattering element, like carbon, presents a great challenge to proper data corrections due to the majority contribution of Compton scattering signal in high Q region. The reduced structure function, $F(Q)$, for $Q_{max} = 25.0$ Å^{-1}, and the corresponding PDF are shown in Fig. 4. A structural model (space group *P63mc*) is refined and gave R_{wp} of 0.32, as we can see from the difference curve below in Fig. 4

Conclusion

The lattice constant, scale factor and isotropic thermal factors were refined, with all the parameters maintaining the symmetry of each space group for each structure type. High quality PDFs can be obtained with $Q_{max} = 30.0$ Å^{-1} (or more) for elements with atomic number Z ($12 \leq Z \leq 48$). However, the data for low-Z elements like C (Z = 6) and extremely high-Z elements like Pb (Z = 82) were difficult to analyze up to $Q_{max} = 30.0$ Å $^{-1}$. The Pb and C data could be analyzed up to $Q_{max} = 25.0$ Å^{-1}and $Q_{max} = 20.0$ Å^{-1}, respectively. Over all the fitting is quite good and satisfactory, indicating that RA-PDF technique can be confidently employed in structural studies of elements with atomic number Z ($12 \leq Z \leq 48$). The elements with low atomic number Z present a great challenge to proper data correction due to the majority contribution of Compton scattering in high Q region. The elements with high atomic number Z, show a contribution of fluorescence signal, which can be very significant when the used X-ray energy is not too far above the elements absorption edge(s).

Acknowledgments

We would like to acknowledge help from Didier Wermeille, Doug Robinson, for help in collecting data. We would also like to acknowledge Dr. Simon Billinge group for the support in obtaining and analyzing the Synchrotron data. This work was supported in part by National Science Foundation (NSF) grant DMR-0304391. Data were collected at the 6IDD beamline of the MUCAT sector at the Advanced Photon Source (APS). Use of the APS is supported by the U.S. DOE, Office of Science, Office of Basic Energy Sciences, under Contract No. W-31-109-Eng-38. The MUCAT sector at the APS is supported by the U.S. DOE, Office of Science, Office of Basic Energy Sciences, through the Ames Laboratory under Contract No. W-7405-Eng-82.

References

[1]Egami, T. and Billinge, S.J.L. " Underneath the Bragg peaks: structural analysis of complex materials", 1st Ed. (Pergamon Press, Elsevier, Oxford, England, 2003).

[2]Billinge, S.J.L. and Kanatzidis, M.G., Chem. Commun. 2004 (2004) 749.

[3]Furukawa, K., Rep. Prog. Phys. 25 (1962) 395.

[4]Wright, A.C., Glass. Phys. Chem. 24 (1998) 148.

[5]Billinge, S.J.L., DiFrancesco, R.G., Kwei, G.H., Neumeier, J.J. and Thompson, J.D., Phys. Rev. Lett. 77 (1996) 715.

[6]Božin, E.S., Billinge, S.J.L., Takagi, H. and Kwei, G.H., Phys. Rev. Lett. 84 (2000) 5856.

[7]Petkov, V., Billinge, S.J.L., Shastri, S.D. and Himmel, B., Phys. Rev. Lett. 85 (2000) 3436.

[8]Petkov, V., Trikalitis, P.N., Božin, E.S., Billinge, S.J.L., Vogt, T. and Kanatzidis, M.G., J. Am. Chem. Soc. 124 (2002) 10157.

[9]Chupas, P.J., Qiu, X., Hanson, J.C., Lee, P.L., Gery, C.P. and Billinge, S.J.L., J. Appl. Crystallogr. 36 (2003) 1342.

[10]Masadeh, A.S., Božin, E.S., Farrow, C.L. and Billinge, S.J.L. Phys. Rev. B, 76 (2007) 115413.

[11]Derakhshan, S., Assoud, A., Dashjav, E., Qiu, X., Billinge, S.J.L. and Kleinke, H., J. Am. Chem. Soc. 126 (2004) 8295.

[12]Atassi, F., Mao, C., Masadeh, A.S. and Byrn, S.R., Journal of Pharm. Sci. 99 (2010) 3684.

[13]Chupas, P.J., Chaudhuri, S., Hanson, J.C., Qiu, X., Lee, P.L., Shastri, S.D., Billinge, S.J.L. and Gery, C.P., J. Am. Chem. Soc. 126 (2004) 4756.

[14]Hammersley, A.P., Svenson, S.O., Hanfland, M. and Hauserman, D., High Pressure Res. 14 (1996) 235.

[15]Qiu, X., Thompson, J.W. and Billinge, S.J.L., J. Appl. Crystallogr. 37 (2004) 678.

[16]Petkov, V., Billinge, S.J.L., Heising, J. and Kanatzidis, M.G., J. Am. Chem. Soc. 122 (2000) 11571.

[17]Petkov, V., Zavalij, P.Y., Lutta, S., Wittingham, M.S., Parvanov, V. and Shastri, S., Phys. Rev. B, 69 (2004) 085410.

[18]Juhas, P., Cherba, D.M., Duxbury, P.M., Punch, W.F. and Billinge, S.J.L., Nature, 440 (2006) 655.

[19]Zhang, H.Z., Gilbert, B., Huang, F. and Banfield, J.F., Nature, 424 (2003) 1025.

[20]Gilbert, B., Huang, F., Zhang, H., Waychunas, G.A. and Banfield, J.F., Science, 305 (2004) 651.

[21]Neder, R.B. and Korsunskiy, V.I., J. Phys.: Condens. Mat. 17 (2005) S125.

[22]Petkov, V., Peng, Y., Williams, G., Huang, B., Tomalia, D. and Ren, Y., Phys. Rev. B, 72 (2005) 195402.

[23]Warren, B.E., “X-ray diffraction”, (Dover, New York, 1990).

[24]Billinge, S.J.L., “Local Structure from Diffraction”, Eds S.J.L. Billinge and M.F. Thorpe, (Plenum, New York, 1998), p. 137.

[25]Rietveld, H.M., J. Appl. Crystallogr. 2 (1969) 65.

[26]Proffen, T. and Billinge, S.J.L., J. Appl. Crystallogr. 32 (1999) 572.

[27]Toby, B.H. and Billinge, S.J.L., Acta Crystallogr. A, 60 (2004) 315.

[28]Toby, B.H. and Egami, T., Acta Crystallogr. A, 48 (1992) 336.

[29]Jeong, I.K., Proffen, T., Mohiuddin-Jacobs, F. and Billinge, S.J.L., J. Phys. Chem. A, 103 (1999) 921.

[30]Jeong, I.K., Heffner, R.H., Graf, M.J. and Billinge, S.J.L., Phys. Rev. B, 67 (2003) 104301.

[31]Hammersley A.P., ESRF Internal Report ESRF98HA01T, (1998).

[32]Zaleski, J., Wu, G. and Coppens, P., J. Appl. Crystallogr. 31 (1998) 302.

[33]Ito, M. and Amemiya, Y., Nuclear Instruments & Methods In Physics Research Section A-Accelerators Spectrometers Detectors And Associated Equipment, 310 (1991) 369.